Non-Reciprocal Metamaterials With Simultaneously Time-Varying Stiffness and Mass

Jiahui Huang
Key Laboratory of Dynamics and Control of Flight Vehicle,
Ministry of Education,
School of Aerospace Engineering,
Beijing Institute of Technology,
Beijing 100081, China
e-mail: huang_jh@bit.edu.cn

Xiaoming Zhou[1]
Key Laboratory of Dynamics and Control of Flight Vehicle,
Ministry of Education,
School of Aerospace Engineering,
Beijing Institute of Technology,
Beijing 100081, China
e-mail: zhxming@bit.edu.cn

A modulated metamaterial that exhibits both time-periodic stiffness and mass simultaneously is presented. The metamaterial element includes a primary body that undergoes infinitesimal motion, and is connected to a dynamic-mechanism structure, involving a rotational body, and spring with a large-scale motion, which is designed to produce a time-modulated linear momentum and elastic constraint for the primary body. The non-reciprocal wave propagation is then investigated in a space–time lattice metamaterial that is constructed by coupling doubly time-modulated elements with linear springs of constant stiffness. The dispersion property shows the frequency degeneracy occurring at the center or edge of the Brillouin zone, and the unidirectional bandgap at certain frequencies. This phenomenon represents a unique property of the doubly modulated metamaterials compared to the singly modulated ones, thus may provide more promising applications to the design of non-reciprocal devices. [DOI: 10.1115/1.4046844]

Keywords: modulated metamaterials, time-periodic mass, time-periodic stiffness, space–time modulation, non-reciprocal wave propagation, dynamics, mechanical properties of materials, wave propagation

1 Introduction

Metamaterials are artificial composite materials engineered to achieve unusual physical properties [1–4]. Metamaterials are usually designed by the periodic arrangement of scattering elements in spatial dimensions, thus maintaining the material properties unchanged with time. In the space-only modulated media, the intrinsic time-reversal symmetry limits the wave propagation to be reciprocal, that is, the response at a receiver from an oscillating source is unchanged regardless of an interchange of their positions. However, the breaking of wave reciprocity [5–14] is highly desirable in scenarios wherein a directive energy transfer in the seismic wave protection, noise insulation, and energy harvesting is required. One of the promising approaches for achieving the non-reciprocity is tailoring the mechanical properties of materials (typically inertial mass and/or stiffness) in both space and time dimensions, as suggested in some of the recent studies [15–29]. When material properties are weakly modulated in space and time domains in a wave-like manner, the spatiotemporal modulation acts like a biasing load that breaks the time-reversal symmetry. The non-reciprocity is manifested by asymmetric bandgaps in the dispersion diagram, which can be calculated using the multiple time scales perturbation theory [30], the Bloch theorem along with the harmonic balance methodology [31], coupled-mode theory [32], theory of field patterns [33], and the generalized plane wave expansion method [34].

The realization of the time-modulated mechanical properties is challenging; usually, external control fields should be introduced to achieve high modulation speed that is comparable to the wave propagation velocity. Recently, the experimental realization of time-periodic stiffness has been reported in a dynamic phononic crystal consisting of permanent magnets modulated by the externally driven coils [35,36], in an elastic waveguide consisting of an array of piezoelectric patches shunted through the negative-capacitance circuits [37], or in an elastic metamaterial beam with the dynamically varied angular orientation of local resonators [38]. Other possible methods for the stiffness modulation include the means of shock waves in soft materials [39], magneto-rheological elastomers [40], and the photo-elastic effect [41]. Still, the above solutions are not well suited for realizing a time-periodic inertial mass. Therefore, a new design approach relying on artificial metamaterials with dynamic-mechanism microstructures was proposed to implement the time modulation of mass [42]. This study demonstrated that the dynamic-mechanism metamaterial could denote a feasible solution for the realization of the mechanical time-varying properties.

The simultaneous space–time modulation of stiffness and mass provides higher freedoms in manipulating the non-reciprocal wave propagation. However, the design of the doubly modulated medium still remains unknown. In this work, we report the design of a structural model of the doubly modulated medium by using the dynamic-mechanism metamaterial. Control of non-reciprocal wave propagation in metamaterials with the simultaneous space–time modulation of stiffness and mass will be studied.

The rest of the paper is organized as follows: in Sec. 2, a doubly modulated metamaterial made of dynamic-mechanism microstructures is presented. In Sec. 3, the spatiotemporal periodic lattice metamaterials with simultaneously modulated mass and stiffness are introduced, and the method for dispersion estimation of the doubly modulated lattice is explained. In Sec. 4, the non-reciprocal wave phenomena induced by the spatiotemporal modulation of mass and stiffness are discussed. Lastly, concluding remarks are outlined in Sec. 5.

2 Metamaterial Elements with Simultaneously Time-Varying Mass and Stiffness

2.1 Model Design. The doubly time-varying metamaterial element is presented in Fig. 1. This element contains a primary body of weight m_0 moving along a motionless slide track and two dynamic mechanisms that are characterized by the rotational structure with a constant angular frequency ω_r, which are arranged on the top and bottom of the m_0-body, respectively. The mechanism positioned on the top of the primary body involves two rotational elastic springs of the rest length l_0 with a tension stiffness K and a shearing

[1]Corresponding author.

Contributed by the Applied Mechanics Division of ASME for publication in the Journal of Applied Mechanics. Manuscript received January 25, 2020; final manuscript received March 31, 2020; published online April 8, 2020. Assoc. Editor: Yashashree Kulkarni.

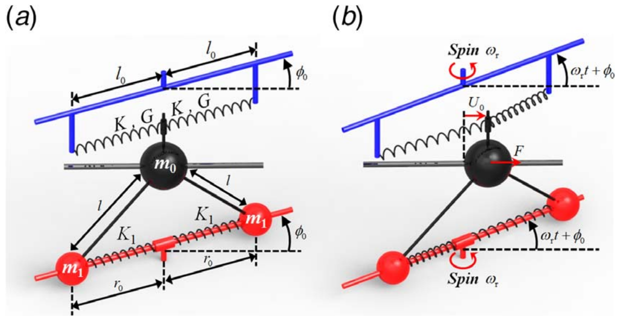

Fig. 1 Schematic diagram of the doubly time-modulated metamaterial element. The elementary cell consists of a rigid body of weight m_0 that is constrained to move along a motionless slide track and two spinning structures, respectively, placed at the top and bottom of the m_0-body. (*a*) At an initial time, the top and bottom structures form an angle ϕ_0 relative to the motionless track, and (*b*) at a later time *t*, this angle becomes $\omega_r t+\phi_0$ due to the rotation of angular frequency ω_r, and the m_0-body undergoes a displacement U_0 when being subject to a force *F*.

one G, and is used to produce the time-periodic elastic constraint to the primary body. The bottom mechanism consists of two rigid bodies of the same weight m_1 residing on a rotational guide track at the equal distance r_0 to the spin center, and is used for creating the periodically time-varying mass in a similar way as presented in Ref. [42]. Two m_1-bodies are pin connected to the m_0-body by rigid and massless bars of length l. A ground spring of a tension stiffness K_1 is added between the m_1-body and spin center for reducing the instability caused by the centrifugal force of rotational bodies, which needs to be taken into account in the high-speed rotation mode. At an initial time, the top and bottom structures form an angle ϕ_0 relative to the motionless track, and this angle becomes $\omega_r t+\phi_0$ at a later time t due to the rotation of angular frequency ω_r, as schematically shown in Fig. 1.

The effective dynamic mass and stiffness of the metamaterial element are defined using the homogenization scheme that relies on the responded displacement U_0 of the m_0-body subject to an arbitrary force F, as illustrated in Fig. 1(*b*). Without considering the gravity of all the bodies, the equilibrium equation of the m_0-body is expressed as

$$F - F_T - F_B = m_0 \ddot{U}_0 \tag{1}$$

where F_T and F_B denote the forces exerted from the rotational springs and bodies, respectively. By establishing the dynamic equilibrium equation for the spinning structure, as given in Appendix A, forces F_T and F_B can be expressed explicitly in terms of the macroscopic fields F and U_0 under an assumption that the amplitude of displacement U_0 is infinitely small compared to the characteristic lengths, e.g., r_0 and l_0. Finally, the relationship between F and U_0 is given by

$$F - K_{\rm eff}(t)U_0 = \frac{\mathrm{d}}{\mathrm{d}t}\left[m_{\rm eff}(t)\frac{\mathrm{d}U_0}{\mathrm{d}t}\right] \tag{2}$$

where $m_{\rm eff}(t)$ and $K_{\rm eff}(t)$ denote the time-dependent functions, which are respectively expressed as

$$m_{\rm eff}(t) = m_0 + 2m_1\cos^2(\omega_r t+\phi_0) \tag{3}$$

$$K_{\rm eff}(t) = 2G + 2(K - G + K_1 - 2m_1\omega_r^2)\cos^2(\omega_r t+\phi_0) \tag{4}$$

According to Eq. (2), the metamaterial element can be equivalently represented by a single body having the time-periodic mass $m_{\rm eff}(t)$ and a connection to the ground spring whose stiffness $K_{\rm eff}(t)$ varies periodically with time. Notice that the term $-4m_1\omega_r^2\cos^2(\omega_r t+\phi_0)$ in $K_{\rm eff}(t)$ arises from a centrifugal force that may cause instability of the m_0-body. Since its resultant effect is equivalent to the ground spring constraint, this term would only bring about the change of effective modulation stiffness. For analytical simplicity, the condition $K_1 = 2m_1\omega_r^2$ is set in our model, but it would not limit the tunability of the dynamic mechanism. Equations (3) and (4) can be further represented in the form of a sum of a constant term and a modulation parameter, so they become

$$m_{\rm eff}(t) = M_0 + M_m\cos(\omega_m t+\Phi_0) \tag{5}$$

$$K_{\rm eff}(t) = K_0 + K_m\cos(\omega_m t+\Phi_0) \tag{6}$$

where $M_0 = m_0 + m_1$, $M_m = m_1$, $K_0 = K+G$, $K_m = K-G$, $\omega_m = 2\omega_r$, and $\Phi_0 = 2\phi_0$.

2.2 Energy Inputted Into System. A boundary condition that the spinning structure is forced to rotate with a constant angular frequency has been assumed for the model. This boundary condition implies that an external moment of force is needed to balance its internal moment caused by the rotational spring and mass so that the total moment acting on the spinning structure is equal to zero. Here, we analyze the input work done by this external moment of force to measure the energy that needs to be input to the system to achieve the time-varying properties. Suppose that the m_0-body undergoes a harmonic oscillation of displacement $U_0(t) = \hat{U}_0\sin(\omega t)$, where $\hat{U}_0$ denotes the oscillation amplitude and ω denotes the oscillation frequency. Then, the external moment of force that maintains constant rotation of both top and bottom structures, denoted as M_T and M_B respectively, can be calculated as given in Appendix B. The total instantaneous power input is calculated as $P_{\rm total} = P_F + P_M$, where P_F and P_M denote the rate of work done by force F acting on the m_0-body and the external moment of force on the spinning structure, respectively. The internal energy $E_{\rm total}$ of the metamaterial element consists of the kinetic energy of rigid bodies, E_k, and the potential energy of springs, E_p, which can be computed by the procedures provided in Appendix B.

Considering the structural parameters $m_0 = 1$ kg, $m_1 = 0.5$ kg, $d = 12$ cm, $l = 20$ cm, $l_0 = r_0 = 16$ cm, $K = 400$N/m, $G = 100$N/m, $\phi_0 = 0$, $\omega_r = 4\pi$ rad/s, and $\omega = 40\pi$ rad/s, the time-domain power input $P_{\rm total}$ and the time rate of change in the internal energy $\mathrm{d}(E_{\rm total})/\mathrm{d}t$ in a rotation period are presented in Fig. 2(*a*). Thus, the energy conservation characterized by $P_{\rm total} = \mathrm{d}(E_{\rm total})/\mathrm{d}t$ can be verified. The external energy input denoted as P_M represents only a small portion of the total energy. Furthermore, the net energy input $W_M = \int_0^t P_M\,\mathrm{d}t$ indicates that the energy first flows into the system and then is extracted, as shown in Fig. 2(*b*). Therefore, for the ideal system with no friction, no damping, no non-conservative forces, zero energy input is required to maintain the constant rotation of

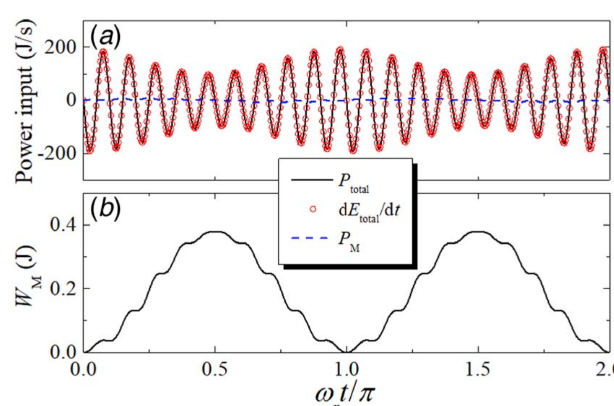

Fig. 2 (*a*) The total instantaneous power input $P_{\rm total}$ and external energy input P_M, as well as the time rate of change in the internal energy $\mathrm{d}(E_{\rm total})/\mathrm{d}t$, and (*b*) the net energy input $W_M = \int_0^t P_M dt$ during one rotation period

dynamic mechanisms. It is worth to point out that this energy-conserved effect has been also recently observed in gyric metamaterials with the angular momentum modulation [43], enabling the system to exhibit a stable response irrespective of the driven frequency.

3 Spatiotemporal Periodic Lattice Metamaterials With Simultaneously Modulated Mass and Stiffness

An infinite periodic lattice metamaterial can be constructed by coupling doubly time-varying elements with linear interactions through springs of constant stiffness. Such a lattice metamaterial is proposed to achieve the spatiotemporal modulation over mass and stiffness simultaneously. In this work, a Bloch-based method is adopted to obtain dispersion diagrams, and to identify the nonreciprocal wave behavior in the numerical examples presented in Sec. 4.

Figure 3(*a*) shows the schematic diagram of the group of doubly time-varying elements, where the m_0-bodies in adjacent elements are connected by springs that have a constant stiffness K_c with a separation distance a. A supercell contains R elements with different initial biasing angles ϕ_0 that produce a spatial modulation with periodicity $\lambda_m = Ra$. According to the effective-medium representation, a dynamic structure can be regarded as a single body with a time-modulated mass and a ground spring, as illustrated in Fig. 3(*b*). Based on Eqs. (5) and (6), the modulated mass and stiffness of the r-th ($r = 1, 2, \ldots, R$) element in a supercell are expressed as

$$m^{(r)}(t) = M_0[1 + \alpha_m \cos(\omega_m t + \Phi_0^{(r)})] \tag{7}$$

$$K^{(r)}(t) = K_0[1 + \beta_m \cos(\omega_m t + \Phi_0^{(r)})] \tag{8}$$

The generalized motion equation of the n-th supercell is expressed as

$$\begin{aligned}\dot{\mathbf{M}}(t)\dot{\mathbf{u}}_n(t) + \mathbf{M}(t)\ddot{\mathbf{u}}_n(t) + \mathbf{K}(t)\mathbf{u}_n(t) + \mathbf{K}^{(n-1)}\mathbf{u}_{n-1}(t) + \mathbf{K}^{(n)}\mathbf{u}_n(t)\\ + \mathbf{K}^{(n+1)}\mathbf{u}_{n+1}(t) = 0\end{aligned} \tag{9}$$

where $\mathbf{u}_n = [u_n^{(1)}, u_n^{(2)}, \ldots, u_n^{(R)}]^{\mathrm{T}}$ is a displacement associated with each element in a supercell; $\mathbf{M}(t)$ and $\mathbf{K}(t)$ denote the time-dependent matrices associated with the time-driven mass and ground spring, respectively; $\mathbf{K}^{(n)}$ denotes a constant stiffness matrix that describes the coupling between the neighboring cells. The dispersion relation of the doubly modulated metamaterial can be estimated by finding a plane wave solution [31,42], which is expressed as

$$\mathbf{u}_n(t) = \mathbf{a}(t)e^{i(\omega t - nk\lambda_m)} \tag{10}$$

where k denotes the wavenumber of the Bloch wave, $\mathbf{a}(t)$ represents the modulated amplitude satisfying the periodic condition $\mathbf{a}(t) = \mathbf{a}(t + T_m)$, where $T_m = 2\pi/\omega_m$. By expanding $\mathbf{a}(t)$ to the Fourier series, we get

$$\mathbf{a}(t) = \sum_{p=-\infty}^{\infty} \mathbf{a}_p e^{ip\omega_m t} \tag{11}$$

From Eq. (10), it can be deduced that

$$\mathbf{u}_{n-1}(t) = e^{i\mu}\mathbf{u}_n(t), \quad \mathbf{u}_{n+1}(t) = e^{-i\mu}\mathbf{u}_n(t) \tag{12}$$

where $\mu = k\lambda_m$ is defined as a normalized wavenumber. Furthermore, substituting Eq. (12) into (9), we get

$$\mathbf{M}(t)\ddot{\mathbf{u}}_n(t) + \dot{\mathbf{M}}(t)\dot{\mathbf{u}}_n(t) + \mathbf{K}(t)\mathbf{u}_n(t) + \mathbf{K}_c(\mu)\mathbf{u}_n(t) = 0 \tag{13}$$

where

$$\mathbf{K}_c(\mu) = \mathbf{K}^{(n-1)}e^{i\mu} + \mathbf{K}^{(n)} + \mathbf{K}^{(n+1)}e^{-i\mu} \tag{14}$$

Considering that mass matrix $\mathbf{M}(t)$ and stiffness matrix $\mathbf{K}(t)$ are periodic functions of time, they can be expanded as Fourier series as follows:

$$\mathbf{M}(t) = \sum_{q=-\infty}^{\infty} \hat{\mathbf{M}}_q e^{iq\omega_m t}, \quad \mathbf{K}(t) = \sum_{q=-\infty}^{\infty} \hat{\mathbf{K}}_q e^{iq\omega_m t} \tag{15}$$

where $\hat{\mathbf{M}}_q$ and $\hat{\mathbf{K}}_q$ denote the Fourier coefficients, which are given by

$$\begin{aligned}\hat{\mathbf{M}}_q &= \frac{1}{T_m}\int_{-T_m/2}^{T_m/2} \mathbf{M}(t)e^{-iq\omega_m t}\,\mathrm{d}t,\\ \hat{\mathbf{K}}_q &= \frac{1}{T_m}\int_{-T_m/2}^{T_m/2} \mathbf{K}(t)e^{-iq\omega_m t}\,\mathrm{d}t\end{aligned} \tag{16}$$

By substituting Eqs. (10), (11), (15), and (16) into (13), and perfoming the harmonic balancing, we finally get that

$$\begin{aligned}\sum_{q=-\infty}^{\infty} -(\omega + p\omega_m)[\omega + (p-q)\omega_m]\hat{\mathbf{M}}_q\mathbf{a}_{p-q}\\ + \sum_{q=-\infty}^{\infty} \hat{\mathbf{K}}_q\mathbf{a}_{p-q} + \mathbf{K}_c(\mu)\mathbf{a}_p = 0\end{aligned} \tag{17}$$

A truncation order P needs to be assigned to p such that $\mathbf{a}_p = 0$ when $|p| > P$ [31]. Eventually, Eq. (17) can be expressed in the form of a quadratic eigenvalue equation as follows:

$$[\omega^2\mathbf{L}_2(\mu) + \omega\mathbf{L}_1(\mu) + \mathbf{L}_0(\mu)]\mathbf{a}_{\text{total}} = 0 \tag{18}$$

where $\mathbf{a}_{\text{total}}$ denote eigenvectors. Matrices $\mathbf{L}_0(\mu)$, $\mathbf{L}_1(\mu)$, and $\mathbf{L}_2(\mu)$ are all related to wavenumber μ. The dispersion relation of the doubly modulated metamaterial is obtained by solving eigenvalue equation (18) for eigenfrequency ω in a given wavenumber μ. The eigenvalue problem in Eq. (18) will yield $R \times (2P+1)$ eigenvalues. Here, the focus is placed on the fundamental dispersion mode ($p = 0$) as it normally contains a large portion of the spectral energy. The procedure to retrieve the fundamental dispersion band is illustrated below. By substitution of Eq. (11) into (10), the displacement of the nth supercell is expressed as $\mathbf{u}_n(t) = \sum_{p=-\infty}^{\infty} \mathbf{a}_p e^{i[(\omega+p\omega_m)t - n\mu]}$. The fundamental dispersion band is characterized by an amplitude that is relevant to the leading term of $p = 0$. It can be determined by weighting the magnitude of $\mathbf{a}_0$ for each branch and setting up a filtering value to avoid plotting of the dispersion bands with little spectral energy.

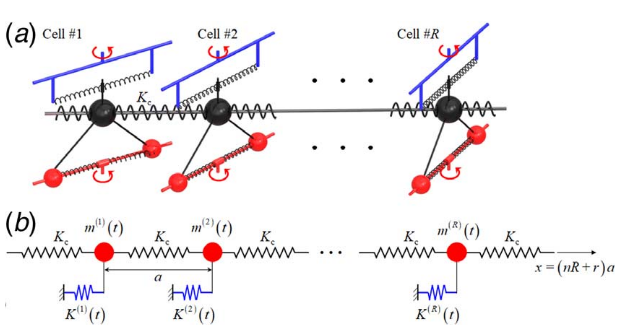

Fig. 3 (*a*) Schematic diagram of the spatiotemporal periodic lattice metamaterial constructed by coupling the doubly time-modulated elements with springs of a constant stiffness K_c. (*b*) The equivalent mass–spring chain model where the time modulation is imposed on the masses and ground springs.

4 Non-reciprocal Wave Phenomena in Doubly Modulated Metamaterials

4.1 Unidirectional Bandgaps and Degeneracy Phenomena. Consider parameters $\omega_m = 0.3\omega_0$, $\alpha_m = 0.2$, $\Phi_0^{(r)} = 2\pi r/3$, and $\eta = K_0/K_c = 1$ of a lattice metamaterial having three elements in a supercell, i.e., $R = 3$, and the corresponding theoretical formulation for the dispersion computation is presented in the Supplementary Material. The analysis of the dispersion diagram of the time-modulated lattice is conducted with reference to the time-invariant case for different modulating amplitudes $\beta_m = 0.2$, 0.4, and 0.8, as displayed in Fig. 4. Note that the dimensionless frequency is defined as $\Omega = \omega/\omega_0$, where $\omega_0 = \sqrt{K_c/M_0}$. In all three cases, the non-modulated lattices exhibit a bandgap from zero to the cutoff frequency because of the Drude dispersion behavior that is caused by the ground boundary condition [44]. Except for this bandgap, the non-modulated lattice with $\beta_m = 0.2$ possesses two additional bandgaps, as shown in Fig. 4(*a*), where the upper and lower gaps open at the center ($\mu = 0$) and edge ($\mu = \pm\pi$) of the first Brillouin zone (BZ), respectively. When the temporal modulation is introduced, each gap splits into two unidirectional bandgaps while the gap bandwidth stays unchanged, as shown in Fig. 4(*d*). The difference in the central frequency between the two split gaps is equal to the modulation frequency, $\omega_m/\omega_0 = 0.3$. Notice that the band structure in the first BZ would repeat itself in other regions beyond the first BZ. This means that the same bandgap frequency shift appears between the bandgaps of different BZs. The similar non-reciprocal phenomenon can be also observed in lattice systems with a single modulation, either mass or stiffness modulation [31,42]. In this work, particular attention is paid to the non-modulated lattices at $\beta_m = 0.4$ or $\beta_m = 0.8$, which show the frequency degeneracy at the BZ edge or BZ center, as illustrated in Figs. 4(*b*) and 4(*c*), respectively. The degeneracy phenomenon can also be observed in the modulated lattices, as shown in Figs. 4(*e*) and 4(*f*), because the time modulation causes only the frequency shifting of bandgaps without altering the bandwidth. As a result, the frequency degeneracy at the BZ edge (center) leads to the disappearance of the lower (upper) unidirectional bandgap, so the non-reciprocity appears only in the upper (lower) bandgaps.

In order to verify the analytical dispersion results, the dispersion diagram is reconstructed from the time-dependent simulation for the doubly modulated lattices presented in Figs. 4(*d*)–4(*f*). In the simulation, the periodic lattice structure is excited with a displacement load characterized by the Gaussian-modulated sinusoidal broadband signal as shown in Fig. 5(*a*). Here, the signal bandwidth is wide enough to cover the frequency range of the dispersion diagram. Figures 5(*b*)–5(*d*) show the band diagram obtained by the normalized amplitude of the Fourier transformed displacement fields in the (μ, Ω) space. The excellent agreement between analytical prediction and time-dependent simulation results can be observed, which validates the analytical Bloch-based method.

The doubly modulated metamaterial with the degeneracy effect may provide more promising applications in design of non-reciprocal devices. One of the perspective applications may be the non-reciprocal bandpass filtering for wave and vibration. For further explanation, Figs. 6(*a*) and 6(*b*) show displacement response spectra in opposite directions for modulated metamaterials without and with the degeneracy effect, which correspond to the models concerned in Figs. 4(*d*) and 4(*e*), respectively. The modulated lattice without the degeneracy effect exhibits asymmetric wave transmission in multiple frequency bands [Fig. 6(*a*)]. By contrast, due to the degeneracy effect, the non-reciprocal wave behavior for the transmission of either the right-travelling or left-travelling wave appears in only one frequency band. This single-band feature may benefit to the design of non-reciprocal bandpass filters, in which the doubly modulated lattice with the degeneracy effect allows waves and vibrations within a selected frequency band and direction to be transmitted while preventing waves at opposite directions from passing on.

In the following, the degeneracy condition is derived by using the dispersion equation of the non-modulated lattice. The equation of motion given by Eq. (13) for the non-modulated lattice at $R = 3$ is

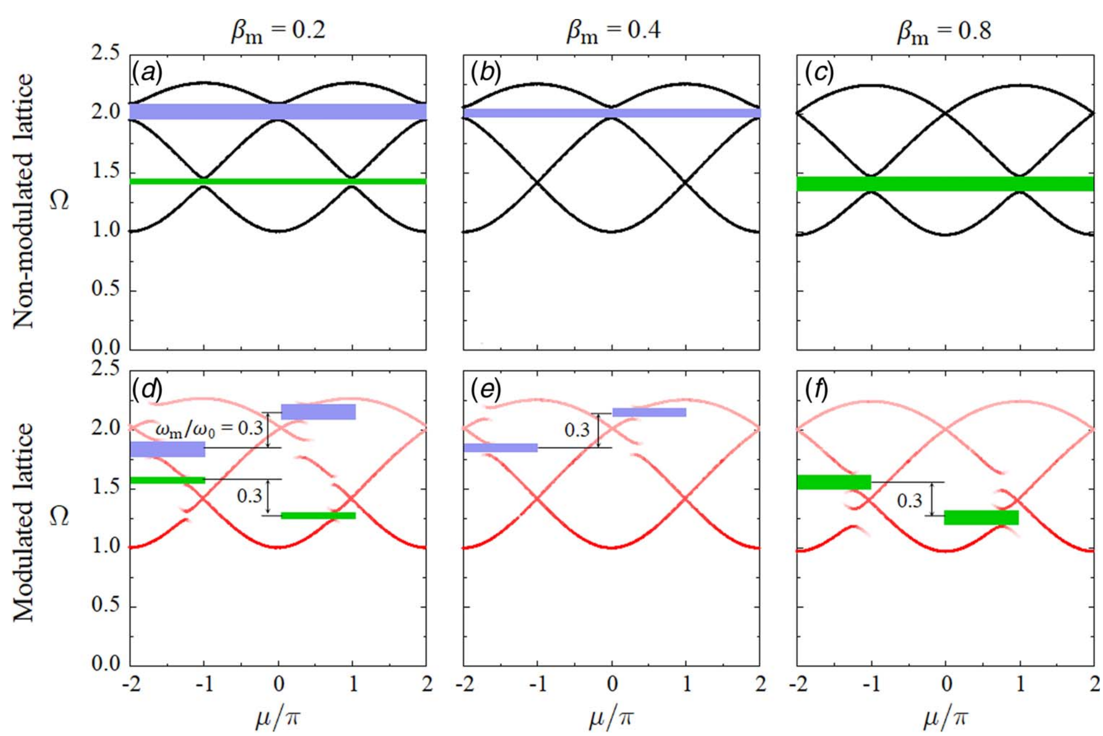

Fig. 4 The dispersion curves of the non-modulated lattice at modulating amplitudes of (*a*) $\beta_m = 0.2$, (*b*) $\beta_m = 0.4$, and (*c*) $\beta_m = 0.8$. The fundamental dispersion branches at $\omega_m = 0.3\omega_0$ of the modulated lattice corresponding to the modulating amplitudes of (*d*) $\beta_m = 0.2$, (*e*) $\beta_m = 0.4$, and (*f*) $\beta_m = 0.8$.

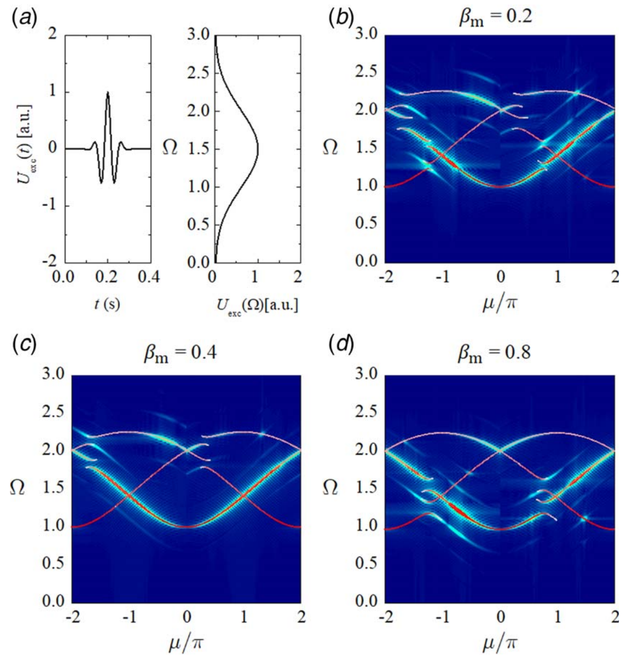

Fig. 5 **(*a*) The displacement excitation spectrum in the time and frequency domain and (*b*–*d*) comparison between the dispersion diagram obtained by the analytic Bloch-based method and reconstruction from the time-dependent simulation for the doubly modulated lattices presented in Figs. 4(*d*)–4(*f*)**

expressed as $\mathbf{B}\mathbf{u}_n(t) = 0$, and the matrix $\mathbf{B}$ follows from

$$\mathbf{B} = K_c[(\eta - \Omega^2)\mathbf{I} + (\eta\beta_m - \Omega^2\alpha_m)\ \mathrm{diag}(-1/2,\ -1/2,\ 1)] + \mathbf{K}_c(\mu) \tag{19}$$

where $\mathbf{I}$ denotes the identity matrix and the symbol "diag" refers to a diagonal matrix in which all off-diagonal components are zero. The stiffness matrix $\mathbf{K}_c(\mu)$ is expressed as

$$\mathbf{K}_c(\mu) = K_c \begin{bmatrix} 2 & -1 & -e^{i\mu} \\ -1 & 2 & -1 \\ -e^{-i\mu} & -1 & 2 \end{bmatrix} \tag{20}$$

To obtain the degeneracy condition such that $\det \mathbf{B} = 0$ has repeated eigenfrequency roots in a given wavenumber μ, we consider the relation

$$\eta\beta_m - \Omega^2\alpha_m = 0 \tag{21}$$

In this case, the matrix $\mathbf{B}$ reduces to $\mathbf{B}^0$, which is given by

$$\mathbf{B}^0 = K_c(\eta - \Omega^2)\mathbf{I} + \mathbf{K}_c(\mu) \tag{22}$$

To obtain the degeneracy condition at the BZ center, $\mu = 0$ is set in Eq. (22), then $\det \mathbf{B}^0 = 0$ leads to

$$(2 + \eta - \Omega^2)^3 - 3(2 + \eta - \Omega^2) - 2 = 0 \tag{23}$$

Equation (23) has a pair of degenerate (repeated) roots, denoted by $\Omega^{\mathrm{deg}} = \sqrt{3 + \eta}$. The combination of the solution $\Omega = \Omega^{\mathrm{deg}}$ and Eq. (21) yield the following condition:

$$\eta\beta_m = (3 + \eta)\alpha_m \tag{24}$$

We note that Eq. (24) refers to the condition for the frequency degeneracy appearing at the BZ center. For verification, substituting the condition (24) into the expression (19) leads to a reduced form of the matrix $\mathbf{B}$, here denoted by $\mathbf{B}'$ as given below

$$\mathbf{B}' = K_c[(\eta - \Omega^2)\mathbf{I} + \alpha_m(3 + \eta - \Omega^2)\ \mathrm{diag}(-1/2,\ -1/2,\ 1)] + \mathbf{K}_c(\mu) \tag{25}$$

Now, let us sweep the frequency to find out Ω that satisfies $\det \mathbf{B}' = 0$. When Ω is equal to $\sqrt{3 + \eta}$, the term with $\alpha_m(3 + \eta - \Omega^2)$ in Eq. (25) vanishes. At this case, $\mathbf{B}'$ reduces to $\mathbf{B}^0$of the form (22). At the BZ center ($\mu = 0$), the equation $\det \mathbf{B}^0 = 0$, or equivalently Eq. (23), has a pair of degenerate roots $\Omega = \Omega^{\mathrm{deg}}$, which is same to the sweeping frequency $\Omega = \sqrt{3 + \eta}$. The result means that the condition (24) ensures the presence of degenerate roots $\Omega = \Omega^{\mathrm{deg}}$. Hence, it expresses the degenerate condition of the BZ center ($\mu = 0$). Similarly, considering Eq. (21), the eigenvalue equation at the edge of first BZ ($\mu = \pm\pi$) can be expressed as

$$(2 + \eta - \Omega^2)^3 - 3(2 + \eta - \Omega^2) + 2 = 0 \tag{26}$$

The degenerate root of Eq. (26) is found to be $\Omega = \sqrt{1 + \eta}$. Combining this root with Eq. (21) we can obtain the degeneracy condition of the BZ edge as follows:

$$\eta\beta_m = (1 + \eta)\alpha_m \tag{27}$$

Based on the fact that the dynamic modulation would not induce the change of the gap bandwidth, Eqs. (24) and (27) also refer to the degeneracy conditions for the modulated lattice.

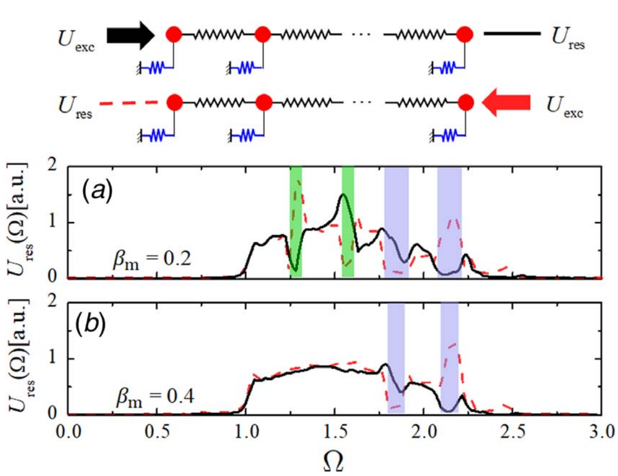

Fig. 6 **The displacement response spectra in opposite directions for modulated metamaterials (*a*) without and (*b*) with the degeneracy effect, which correspond to the models concerned in Figs. 4(*d*) and 4(*e*), respectively**

4.2 Gap Bandwidth Under Frequency Degeneracy.

A wide frequency bandwidth of the non-reciprocal bandgap is desirable in device applications. In this section, we study how to widen the bandgap on the condition that the degeneracies are happening. A theoretical estimation of the gap bandwidth is conducted based on the non-modulated lattice. We first examine the bandwidth of the lower-only bandgap that is created by making a degeneracy at the BZ center. By substituting the degeneracy condition (24) into Eq. (19), we get the eigenvalue equation at the BZ edge, which is given by

$$\left[x - \frac{1}{2}\alpha_m(x + 1) - 1\right]\left\{\left[x - \frac{1}{2}\alpha_m(x + 1) + 1\right][x + \alpha_m(x + 1)] - 2\right\} = 0 \tag{28}$$

where $x(\Omega) = 2 + \eta - \Omega^2$. Solving Eq. (28) for the start and end frequencies of the lower bandgap, we obtain

$$\Omega_1^{\mathrm{gap},\pi} = \sqrt{1 + \eta - A}, \quad \Omega_2^{\mathrm{gap},\pi} = \sqrt{3 + \eta - B} \tag{29}$$

where $A = 2\alpha_m/(2 - \alpha_m)$ and $B = \left[1 + \sqrt{3(5\alpha_m + 6)/(2 - \alpha_m)}\right]/[2(\alpha_m + 1)]$. To evaluate the bandwidth of the upper-only bandgap, we substitute the degeneracy condition (27) into Eq. (19) to obtain the eigenvalue equation at the BZ center, which is expressed as

$$\left[x-\frac{1}{2}\alpha_{\mathrm{m}}(x-1)+1\right]\left\{\left[x-\frac{1}{2}\alpha_{\mathrm{m}}(x-1)-1\right][x+\alpha_{\mathrm{m}}(x-1)]-2\right\}=0 \tag{30}$$

The start and end frequencies of the upper bandgap, denoted as $\Omega_1^{\mathrm{gap},0}$ and $\Omega_2^{\mathrm{gap},0}$, can be obtained by Eq. (30), and they are given by

$$\Omega_1^{\mathrm{gap},0}=\sqrt{1+\eta+B},\quad \Omega_2^{\mathrm{gap},0}=\sqrt{3+\eta+A} \tag{31}$$

The gap edge frequencies of the non-modulated lattice at various modulating amplitude α_{m} but at constant stiffness ratio of $\eta=1$ are presented in Figs. 7(*a*) and 7(*c*). It should be noted that β_{m} can be determined from the degeneracy condition once the values of α_{m} and η are given. The results show that the bandwidth of either upper or lower bandgap (as shaded) can be widened by increasing the value of α_{m}, while the gap center frequency is nearly unchanged with the variation in α_{m}. The changing trends of the gap edge frequencies with the value of η at a constant modulating amplitude of $\alpha_{\mathrm{m}}=0.2$ are presented in Figs. 7(*b*) and 7(*d*), where it can be seen that the bandgap frequency can be enhanced by increasing η, and the bandwidth is insensitive to the change in the η value.

To verify the prediction of the non-modulated lattice, Fig. 8 plots the fundamental dispersion branch of the corresponding modulated lattice at $\omega_{\mathrm{m}}=0.3\omega_0$ for three different values of α_{m}: (*a*, *d*) $\alpha_{\mathrm{m}}=0.1$, (*b*, *e*) $\alpha_{\mathrm{m}}=0.15$, and (*c*, *f*) $\alpha_{\mathrm{m}}=0.2$. The other parameters are the same as those in Fig. 7. In Fig. 8, it is seen that the bandwidth of the unidirectional bandgap can be widened with the increase in α_{m}, while the gap center frequency is almost unchanged, which is in agreement with the results presented in Figs. 7(*a*) and 7(*c*). The effect of the stiffness ratio η on the bandwidth of the unidirectional bandgap is also evaluated as plotted in Fig. 9 in three cases: (*a*, *d*) $\eta=1$, (*b*, *e*) $\eta=2$, and (*c*, *f*) $\eta=3$. The results show that with the increase in the stiffness ratio η, the bandwidth of the unidirectional bandgap shows a small change in bandwidth, but it shifts to higher frequencies, which is in accordance with the results presented in Figs. 7(*b*) and 7(*d*).

5 Conclusion

The modulated media, whose mechanical properties are changed in both space and time, support the non-reciprocal wave propagation, which is expected to bring the new application possibilities in the field of unprecedented wave and vibration control. However, the realization of time-varying properties poses a great challenge to future applications of modulated media. Although there are many promising methods for stiffness modulation, such as the use of permanent magnets with externally driven coils [35] and piezoelectric patches shunted with circuits [37], and others [38], there has been no general method to create the time-periodic inertial mass yet. To solve this problem, the authors proposed a feasible method for the design of time-varying mass media based on the metamaterials using their microstructures involving dynamic mechanisms [42]. In this paper, a dynamic-mechanism metamaterial with the simultaneous modulation of stiffness and mass is introduced and analyzed through the extensive study on the previously proposed time-varying mass metamaterial. The homogenization scheme is established based on the rigorous theoretical analysis of structural dynamics, explaining that the proposed metamaterial can be represented as a homogeneous body with the simultaneous time-periodic stiffness and mass. The energy input required for this "dynamic" structure is also examined, and it is found that the external energy input denotes only a small portion of the total energy.

By connecting the doubly modulated elements with springs of a constant stiffness, a space–time lattice metamaterial is constructed for manipulation of the non-reciprocal wave propagation. The Bloch-based method is used to obtain the dispersion diagram of doubly modulated lattices. The dispersion diagram shows the presence of asymmetric bandgaps, which is indicative of the wave non-reciprocity. In particular, it is found that the frequency degeneracy appears at the BZ edge or BZ center, causing a unidirectional bandgap at either upper-only or lower-only frequencies.

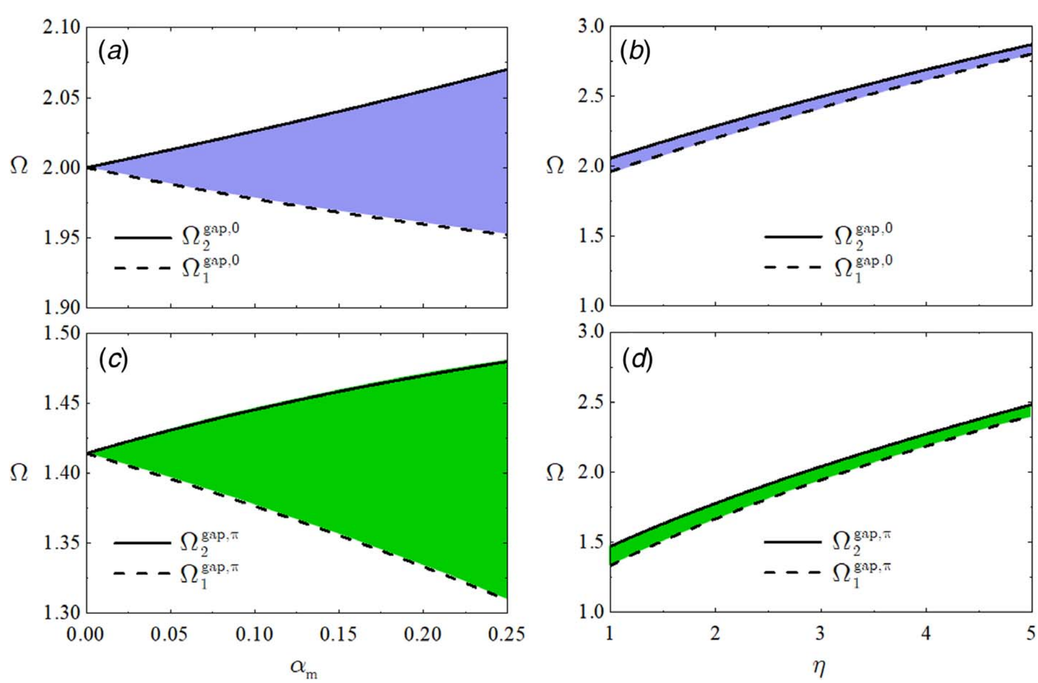

Fig. 7 The start and end frequencies of (*a*) upper-only and (*c*) lower-only bandgaps of the non-modulated lattice at a different modulating amplitude α_{m} and (*b*, *d*) corresponding results for a different stiffness ratio η

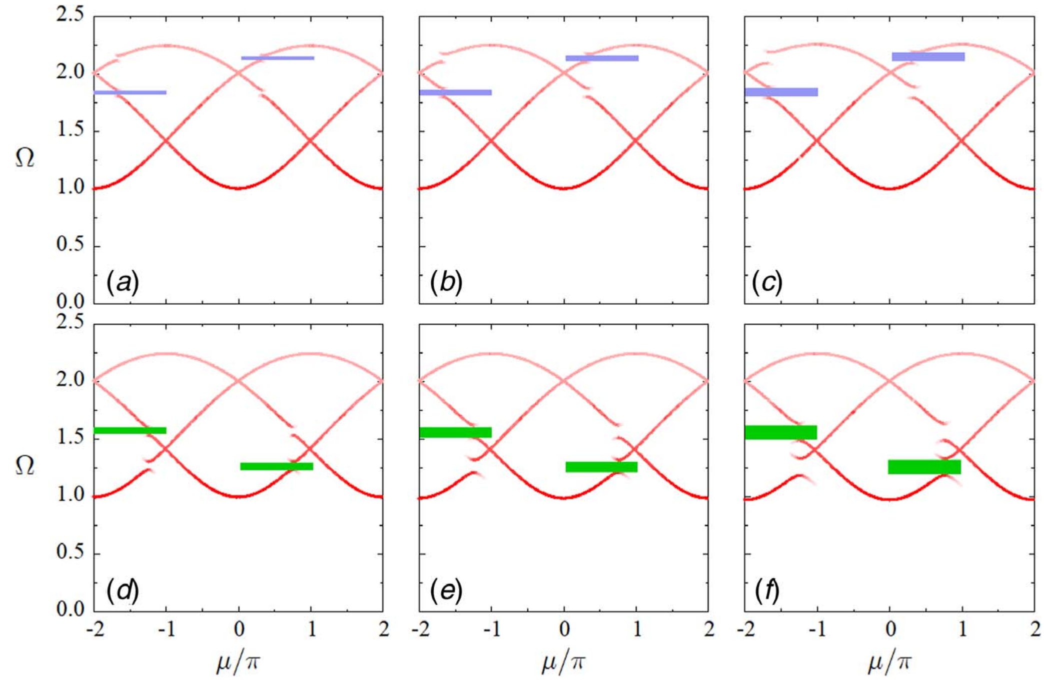

Fig. 8 The fundamental dispersion branch of the modulated lattice with the upper-only bandgap in case of different modulating amplitude: (*a*) $\alpha_\mathrm{m} = 0.1$, (*b*) $\alpha_\mathrm{m} = 0.15$, (*c*) $\alpha_\mathrm{m} = 0.2$, and (*d–f*) corresponding results for the lower-only bandgap

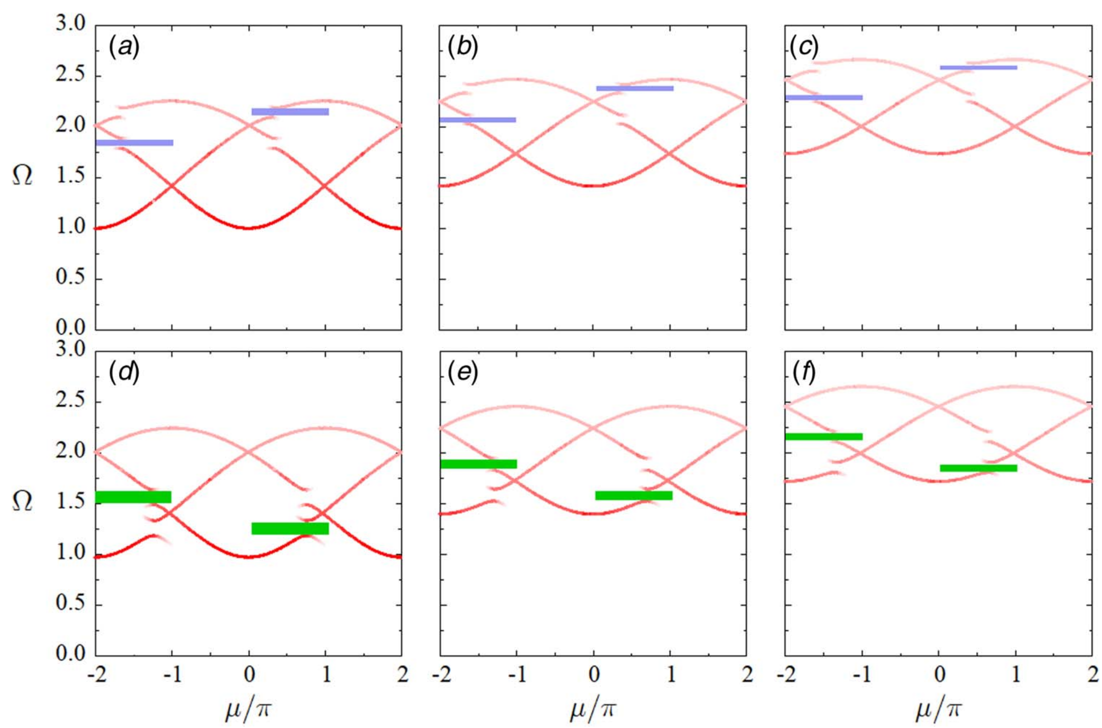

Fig. 9 The fundamental dispersion branch of the modulated lattice with the upper-only bandgap at the different stiffness ratio of (*a*) $\eta = 1$, (*b*) $\eta = 2$, (*c*) $\eta = 3$, and (*d–f*) corresponding results for the lower-only bandgap

The degeneracy condition is derived from the dispersion equation of the non-modulated lattice, and by numerical examples, it is verified that this condition is applicable to the modulated lattice. The influence of the modulating amplitude α_m and stiffness ratio η on the bandwidth of the unidirectional bandgap is also studied, and it is found that by increasing α_m, the bandwidth can be widened, while the gap center frequency stays almost unchanged. In contrast, an increase in η can enhance the gap center frequency, while the bandwidth is almost unchanged. Compared to the singly modulated lattices, the doubly modulated metamaterial can realize the frequency-selective non-reciprocity by making a degeneracy at either the BZ center or the BZ edge, and thus denotes a more promising material for the design of non-reciprocal devices.

Acknowledgment

This work was supported by the National Natural Science Foundation of China [Grant Nos. 11872111, 11991030, 11991033, 11622215, 11521062, and 11572039] and 111 project [Grant No. B16003].

Appendix A: Dynamic Analysis of Doubly Time-Modulated Structure

In Eq. (1), force F_T exerted by the rotational spring is expressed as

$$F_T = F_1^{(K)}\cos\varphi_1^{(K)} + F_1^{(G)}\sin\varphi_1^{(K)} + F_2^{(K)}\cos\varphi_2^{(K)} + F_2^{(G)}\sin\varphi_2^{(K)} \tag{A1}$$

where $F_1^{(K)}$, $F_1^{(G)}$, $F_2^{(K)}$, and $F_2^{(G)}$ represent the forces associated with the tension and shear stiffness of springs #1 and #2, respectively. According to Hooke's law, these forces are expressed as

$$F_1^{(K)} = F_2^{(K)} = KU_0\cos(\omega_r t + \phi_0) \tag{A2}$$

$$F_1^{(G)} = F_2^{(G)} = GU_0\sin(\omega_r t + \phi_0) \tag{A3}$$

Angles $\varphi_1^{(K)} = \angle CAD$ and $\varphi_2^{(K)} = \angle BAE$, as shown in Fig. 10, satisfy the following geometric relationships:

$$\sin\varphi_1^{(K)} = \frac{l_0\sin(\omega_r t + \phi_0)}{l_1},\quad \cos\varphi_1^{(K)} = \frac{l_0\cos(\omega_r t + \phi_0) + U_0}{l_1}, \tag{A4}$$

$$\sin\varphi_2^{(K)} = \frac{l_0\sin(\omega_r t + \phi_0)}{l_2},\quad \cos\varphi_2^{(K)} = \frac{l_0\cos(\omega_r t + \phi_0) - U_0}{l_2}, \tag{A5}$$

where l_1 and l_2 denote the lengths of the deformed springs and can be, respectively, calculated by

$$l_1 = \sqrt{[l_0\cos(\omega_r t + \phi_0) + U_0]^2 + [l_0\sin(\omega_r t + \phi_0)]^2} \tag{A6}$$

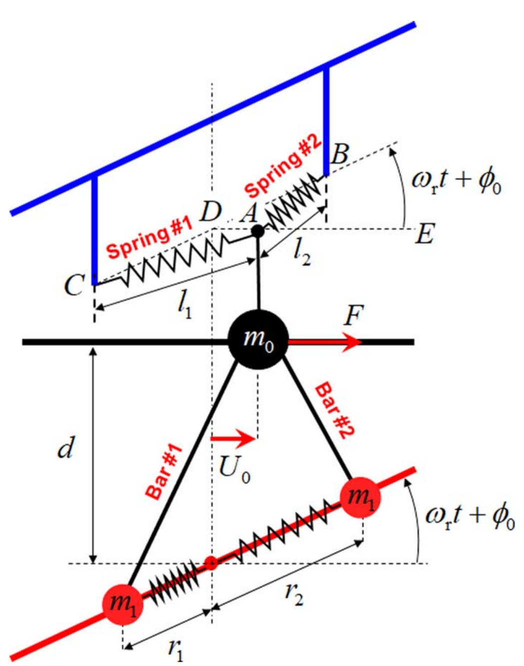

Fig. 10 A schematic view of the geometric configuration of the doubly time-modulated structure

$$l_2 = \sqrt{[l_0\cos(\omega_r t + \phi_0) - U_0]^2 + [l_0\sin(\omega_r t + \phi_0)]^2} \tag{A7}$$

Substitution of Eqs. (A2)–(A5) into (A1) yields

$$\begin{aligned} F_T = {} & [G\sin^2(\omega_r t + \phi_0) + K\cos^2(\omega_r t + \phi_0)]\left(\frac{1}{l_1} + \frac{1}{l_2}\right)U_0 l_0 \\ & + K\cos(\omega_r t + \phi_0)\left(\frac{1}{l_1} - \frac{1}{l_2}\right)U_0^2 \end{aligned} \tag{A8}$$

Force F_B exerted by the rotational m_1-body is expressed as

$$F_B = F_1^{(m)}\cos\varphi_1^{(m)} + F_2^{(m)}\cos\varphi_2^{(m)} \tag{A9}$$

where $F_1^{(m)}$ and $F_2^{(m)}$, respectively, denote the forces in bars #1 and #2, and they are expressed as

$$F_1^{(m)} = \frac{m_1(-\ddot{r}_1 + \omega_r^2 r_1) + K_1(r_0 - r_1)}{r_1 + U_0\cos(\omega_r t + \phi_0)}l \tag{A10}$$

$$F_2^{(m)} = \frac{m_1(\ddot{r}_2 - \omega_r^2 r_2) + K_1(r_2 - r_0)}{r_2 - U_0\cos(\omega_r t + \phi_0)}l \tag{A11}$$

$\varphi_1^{(m)}$ and $\varphi_2^{(m)}$, respectively, denote the included angles between the bar #1 and motionless slide track, and between the bar #2 and motionless slide track, and they satisfy the following geometric relationships:

$$\cos\varphi_1^{(m)} = \frac{r_1\cos(\omega_r t + \phi_0) + U_0}{l} \tag{A12}$$

$$\cos\varphi_2^{(m)} = \frac{r_2\cos(\omega_r t + \phi_0) - U_0}{l} \tag{A13}$$

Furthermore, distances r_1 and r_2 between the m_1-bodies and spinning center satisfy the following geometric relationships:

$$U_0^2 + r_1^2 + 2r_1U_0\cos(\omega_r t + \phi_0) = l^2 - d^2 \tag{A14}$$

$$U_0^2 + r_2^2 - 2r_2U_0\cos(\omega_r t + \phi_0) = l^2 - d^2 \tag{A15}$$

where d refers to the vertical distance from the spinning center of the bottom track to the motionless track.

Based on Eqs. (A8), (A9), (A14) and (A15), and assuming that the magnitude of U_0 is infinitesimal compared to l_0 and r_0, i.e., U_0/l_0, $U_0/r_0 \ll 1$. The equilibrium equation (1) of the m_0-body can be expressed in terms of F and U_0 as follows:

$$\begin{aligned} & F - [2G + 2(K - G)\cos^2(\omega_r t + \phi_0)]U_0 \\ & -2(K_1 - 2m_1\omega_r^2)\cos^2(\omega_r t + \phi_0)U_0 \\ & = [m_0 + 2m_1\cos^2(\omega_r t + \phi_0)]\ddot{U}_0 \\ & \quad -4m_1\omega_r\sin(\omega_r t + \phi_0)\cos(\omega_r t + \phi_0)\dot{U}_0 \end{aligned} \tag{A16}$$

which is equivalent to Eq. (2).

Appendix B: Energy Calculation of the Doubly Time-Modulated Structure

Assuming the displacement response of $U_0(t) = \hat{U}_0\sin(\omega t)$, then force $F(t)$ acting on the m_0 body can be calculated by Eq. (2), which is given by

$$F = m_{\text{eff}}(t)\ddot{U}_0 + \dot{m}_{\text{eff}}(t)\dot{U}_0 + K_{\text{eff}}(t)U_0 \tag{B1}$$

The rate of work done by force $F(t)$, denoted as $P_F(t)$, can be calculated by

$$P_F(t) = F(t)\mathrm{d}U_0(t)/\mathrm{d}t \tag{B2}$$

The moment of force $M_T(t)$ for maintaining a constant rotation of the top spinning structure is determined by the equilibrium equation, which can be expressed as

$$M_T(t) + U_0 \sin(\omega_r t + \phi_0)\left(\frac{F_1^{(K)}}{l_1} + \frac{F_2^{(K)}}{l_2}\right)l_0 + F_2^{(G)}l_2 - F_1^{(G)}l_1 = 0 \tag{B3}$$

where $F_1^{(K)}$, $F_2^{(K)}$, $F_1^{(G)}$, and $F_2^{(G)}$ are calculated by Eqs. (A2) and (A3). The equilibrium equation of the bottom spinning structure that governs the moment of force $M_B(t)$ can be expressed as

$$M_B + \frac{U_0 \sin(\omega_r t + \phi_0)}{l}(F_1^{(m)} r_1 + F_2^{(m)} r_2) - 2m_1\omega_r(r_1\dot{r}_1 + r_2\dot{r}_2) = 0 \tag{B4}$$

where $F_1^{(m)}$ and $F_2^{(m)}$ are calculated by Eqs. (A10) and (A11). The rate of the net work done by the external moment of force is obtained by

$$P_M(t) = \omega_r(M_T + M_B) \tag{B5}$$

The kinetic energies of the m_0-body and m_1-bodies are expressed respectively as

$$E_0 = \frac{1}{2}m_0\omega^2\hat{U}_0^2\cos^2(\omega t) \tag{B6}$$

$$E_1 = \frac{1}{2}m_1(\dot{r}_1^2 + \dot{r}_2^2) + \frac{1}{2}m_1\omega_r^2(r_1^2 + r_2^2) \tag{B7}$$

The time rate of change of the total kinetic energy ($E_k = E_0 + E_1$) is given by

$$\begin{aligned}\mathrm{d}(E_k)/\mathrm{d}t = &-m_0\omega^3\hat{U}_0^2\cos(\omega t)\sin(\omega t) + m_1(\dot{r}_1\ddot{r}_1 + \dot{r}_2\ddot{r}_2)\\ &+ m_1\omega_r^2(r_1\dot{r}_1 + r_2\dot{r}_2)\end{aligned} \tag{B8}$$

where r_1, r_2 and their time derivatives can be computed by Eqs. (A14) and (A15). The potential energies of springs that are characterized by stiffness K, G, and K_1 are expressed, respectively, as

$$E_p^{(K)} = K[\hat{U}_0\sin(\omega t)\cos(\omega_r t + \phi_0)]^2 \tag{B9}$$

$$E_p^{(G)} = G[\hat{U}_0\sin(\omega t)\sin(\omega_r t + \phi_0)]^2 \tag{B10}$$

$$E_p^{(K_1)} = \frac{1}{2}K_1(r_1 - r_0)^2 + \frac{1}{2}K_1(r_2 - r_0)^2 \tag{B11}$$

The time rate of change in the total potential energy ($E_p = E_p^{(K)} + E_p^{(G)} + E_p^{(K_1)}$) is given by

$$\mathrm{d}(E_p)/\mathrm{d}t = \mathrm{d}(E_p^{(K)})/\mathrm{d}t + \mathrm{d}(E_p^{(G)})/\mathrm{d}t + \mathrm{d}(E_p^{(K_1)})/\mathrm{d}t \tag{B12}$$

where

$$\begin{aligned}&\mathrm{d}(E_p^{(K)})/\mathrm{d}t\\ &= K\hat{U}_0^2[\omega\sin(2\omega t)\cos^2(\omega_r t + \phi_0) - \omega_r\sin^2(\omega t)\sin(2\omega_r t + 2\phi_0)]\end{aligned} \tag{B13}$$

$$\begin{aligned}&\mathrm{d}(E_p^{(G)})/\mathrm{d}t\\ &= G\hat{U}_0^2[\omega\sin(2\omega t)\sin^2(\omega_r t + \phi_0) + \omega_r\sin^2(\omega t)\cos(2\omega_r t + 2\phi_0)]\end{aligned} \tag{B14}$$

$$\mathrm{d}(E_p^{(K_1)})/\mathrm{d}t = K_1(r_1 - r_0)\dot{r}_1 + K_1(r_2 - r_0)\dot{r}_2 \tag{B15}$$

Finally, the time rate of change in the internal energy is calculated as

$$\mathrm{d}(E_{\mathrm{total}})/\mathrm{d}t = \mathrm{d}(E_k)/\mathrm{d}t + \mathrm{d}(E_p)/\mathrm{d}t \tag{B16}$$

References

[1] Liu, Z., Zhang, X., Mao, Y., Zhu, Y. Y., Yang, Z., Chan, C. T., and Sheng, P., 2000, "Locally Resonant Sonic Materials," Science, **289**(5485), pp. 1734–1736.

[2] Christensen, J., Kadic, M., Kraft, O., and Wegener, M., 2015, "Vibrant Times for Mechanical Metamaterials," MRS Commun., **5**(3), pp. 453–462.

[3] Ma, G., and Sheng, P., 2016, "Acoustic Metamaterials: From Local Resonances to Broad Horizons," Sci. Adv., **2**(2), p. e1501595.

[4] Cummer, S. A., Christensen, J., and Alù, A., 2016, "Controlling Sound with Acoustic Metamaterials," Nat. Rev. Mater., **1**(3), p. 16001.

[5] Fleury, R., Sounas, D. L., Haberman, M. R., and Alù, A., 2015, "Nonreciprocal Acoustics," Acoust. Today, **11**(3), pp. 14–21.

[6] Fink, M., Cassereau, D., Derode, A., Prada, C., Roux, P., Tanter, M., Thomas, J.-L., and Wu, F., 2000, "Time-reversed Acoustics," Rep. Prog. Phys., **63**(12), pp. 1933–1995.

[7] Zhu, X., Ramezani, H., Shi, C., Zhu, J., and Zhang, X., 2014, "PT-Symmetric Acoustics," Phys. Rev. X, **4**(3), p. 031042.

[8] Popa, B.-I., and Cummer, S. A., 2014, "Non-reciprocal and Highly Nonlinear Active Acoustic Metamaterials," Nat. Commun., **5**(1), p. 3398.

[9] Liang, B., Guo, X. S., Tu, J., Zhang, D., and Cheng, J. C., 2010, "An Acoustic Rectifier," Nat. Mater., **9**(12), pp. 989–992.

[10] Gu, Z.-m., Hu, J., Liang, B., Zou, X.-y., and Cheng, J.-c., 2016, "Broadband Non-Reciprocal Transmission of Sound with Invariant Frequency," Sci. Rep., **6**(1), p. 19824.

[11] Fleury, R., Sounas, D. L., Sieck, C. F., Haberman, M. R., and Alù, A., 2014, "Sound Isolation and Giant Linear Nonreciprocity in a Compact Acoustic Circulator," Science, **343**(6170), pp. 516–519.

[12] Baz, A., 2018, "Active Nonreciprocal Acoustic Metamaterials Using a Switching Controller," J. Acoust. Soc. Am., **143**(3), pp. 1376–1384.

[13] Mojahed, A., Bunyan, J., Tawfick, S., and Vakakis, A. F., 2019, "Tunable Acoustic Nonreciprocity in Strongly Nonlinear Waveguides with Asymmetry," Phys. Rev. Appl., **12**(3), p. 034033.

[14] Leamy, M. J., Darabi, A., Fang, L., Fronk, M., and Vakakis, A., 2019, "Passive Non-reciprocity in Asymmetrical, Hierarchical, Nonlinear Metamaterials," J. Acoust. Soc. Am., **145**(3), pp. 1725–1725.

[15] Trainiti, G., and Ruzzene, M., 2016, "Non-reciprocal Elastic Wave Propagation in Spatiotemporal Periodic Structures," New J. Phys., **18**(8), p. 083047.

[16] Nassar, H., Xu, X. C., Norris, A. N., and Huang, G. L., 2017, "Modulated Phononic Crystals: Non-reciprocal Wave Propagation and Willis Materials," J. Mech. Phys. Solids, **101**, pp. 10–29.

[17] Wallen, S. P., and Haberman, M. R., 2019, "Nonreciprocal Wave Phenomena in Spring-Mass Chains with Effective Stiffness Modulation Induced by Geometric Nonlinearity," Phys. Rev. E, **99**(1), p. 013001.

[18] Yi, K., Collet, M., and Karkar, S., 2017, "Frequency Conversion Induced by Time-Space Modulated Media," Phys. Rev. B, **96**(10), p. 104110.

[19] Ansari, M. H., Attarzadeh, M. A., Nouh, M., and Karami, M. A., 2018, "Application of Magnetoelastic Materials in Spatiotemporally Modulated Phononic Crystals for Nonreciprocal Wave Propagation," Smart Mater. Struct., **27**(1), p. 015030.

[20] Nassar, H., Chen, H., Norris, A. N., and Huang, G. L., 2017, "Non-reciprocal Flexural Wave Propagation in a Modulated Metabeam," Extreme Mech. Lett., **15**, pp. 97–102.

[21] Yi, K., Ouisse, M., Sadoulet-Reboul, E., and Matten, G., 2019, "Active Metamaterials with Broadband Controllable Stiffness for Tunable Band Gaps and non-Reciprocal Wave Propagation," Smart Mater. Struct., **28**(6), p. 065025.

[22] Shui, L.-Q., Yue, Z.-F., Liu, Y.-S., Liu, Q.-C., Guo, J.-J., and He, X.-D., 2015, "Novel Composites with Asymmetrical Elastic Wave Properties," Compos. Sci. Technol., **113**(Supplement C), pp. 19–30.

[23] Nanda, A., and Karami, M. A., 2018, "One-way Sound Propagation via Spatio-Temporal Modulation of Magnetorheological Fluid," J. Acoust. Soc. Am., **144**(1), pp. 412–420.

[24] Yi, K., Collet, M., and Karkar, S., 2018, "Reflection and Transmission of Waves Incident on Time-Space Modulated Media," Phys. Rev. B, **98**(5), p. 054109.

[25] Yi, K., Karkar, S., and Collet, M., 2018, "One-Way Energy Insulation Using Time-Space Modulated Structures," J. Sound Vib., **429**, pp. 162–175.

[26] Lurie, K. A., 2007, *An Introduction to the Mathematical Theory of Dynamic Materials*, Springer, New York, NY.

[27] Cassedy, E. S., and Oliner, A. A., 1963, "Dispersion Relations in Time-Space Periodic Media: Part I-Stable Interactions," Proc. IEEE, **51**(10), pp. 1342–1359.

[28] Cassedy, E. S., 1967, "Dispersion Relations in Time-Space Periodic Media: Part II-Unstable Interactions," Proc. IEEE, **55**(7), pp. 1154–1168.

[29] Attarzadeh, M. A., and Nouh, M., 2018, "Non-reciprocal Elastic Wave Propagation in 2D Phononic Membranes with Spatiotemporally Varying Material Properties," J. Sound Vib., **422**, pp. 264–277.

[30] Swinteck, N., Matsuo, S., Runge, K., Vasseur, J. O., Lucas, P., and Deymier, P. A., 2015, "Bulk Elastic Waves with Unidirectional Backscattering-Immune Topological States in a Time-Dependent Superlattice," J. Appl. Phys., **118**(6), p. 063103.

[31] Vila, J., Pal, R. K., Ruzzene, M., and Trainiti, G., 2017, "A Bloch-Based Procedure for Dispersion Analysis of Lattices with Periodic Time-Varying Properties," J. Sound Vib., **406**(Supplement C), pp. 363–377.
[32] Nassar, H., Chen, H., Norris, A. N., Haberman, M. R., and Huang, G. L., 2017, "Non-reciprocal Wave Propagation in Modulated Elastic Metamaterials," Proc. R. Soc. A: Math. Phys. Eng. Sci., **473**(2202), p. 20170188.
[33] Milton, G. W., and Mattei, O., 2017, "Field Patterns: a new Mathematical Object," Proc. R. Soc. A: Math. Phys. Eng. Sci., **473**(2198), p. 20160819.
[34] Riva, E., Marconi, J., Cazzulani, G., and Braghin, F., 2019, "Generalized Plane Wave Expansion Method for non-Reciprocal Discretely Modulated Waveguides," J. Sound Vib., **449**, pp. 172–181.
[35] Wang, Y., Yousefzadeh, B., Chen, H., Nassar, H., Huang, G., and Daraio, C., 2018, "Observation of Nonreciprocal Wave Propagation in a Dynamic Phononic Lattice," Phys. Rev. Lett., **121**(19), p. 194301.
[36] Chen, Y., Li, X., Nassar, H., Norris, A. N., Daraio, C., and Huang, G., 2019, "Nonreciprocal Wave Propagation in a Continuum-Based Metamaterial with Space-Time Modulated Resonators," Phys. Rev. Appl., **11**(6), p. 064052.
[37] Trainiti, G., Xia, Y., Marconi, J., Cazzulani, G., Erturk, A., and Ruzzene, M., 2019, "Time-Periodic Stiffness Modulation in Elastic Metamaterials for Selective Wave Filtering: Theory and Experiment," Phys. Rev. Lett., **122**(12), p. 124301.
[38] Attarzadeh, M. A., Callanan, J., and Nouh, M., 2020, "Experimental Observation of Nonreciprocal Waves in a Resonant Metamaterial Beam," Phys. Rev. Appl., **13**(2), p. 021001.
[39] Reed, E. J., Soljacic, M., and Joannopoulos, J. D., 2003, "Reversed Doppler Effect in Photonic Crystals," Phys. Rev. Lett., **91**(13), p. 133901.
[40] Danas, K., Kankanala, S. V., and Triantafyllidis, N., 2012, "Experiments and Modeling of Iron-Particle-Filled Magnetorheological Elastomers," J. Mech. Phys. Solids, **60**(1), pp. 120–138.
[41] Gump, J., Finkler, I., Xia, H., Sooryakumar, R., Bresser, W. J., and Boolchand, P., 2004, "Light-Induced Giant Softening of Network Glasses Observed Near the Mean-Field Rigidity Transition," Phys. Rev. Lett., **92**(24), p. 245501.
[42] Huang, J., and Zhou, X., 2019, "A Time-Varying Mass Metamaterial for non-Reciprocal Wave Propagation," Int. J. Solids Struct., **164**, pp. 25–36.
[43] Attarzadeh, M. A., Maleki, S., Crassidis, J. L., and Nouh, M., 2019, "Non-reciprocal Wave Phenomena in Energy Self-Reliant Gyric Metamaterials," J. Acoust. Soc. Am., **146**(1), pp. 789–801.
[44] Yao, S., Zhou, X., and Hu, G., 2010, "Investigation of the Negative-Mass Behaviors Occurring Below a cut-off Frequency," New J. Phys., **12**(10), p. 103025.